11th World Congress on Structural and Multidisciplinary Optimization
7th - 12th, June 2015, Sydney Australia

Multidisciplinary Design Optimization of an Aero-Engine Fan Blade with Consideration of Bypass and Core Performance

Christopher Chahine[1,2], Tom Verstraete[3], Li He[4]

[1] Von Karman Institute for Fluid Dynamics, Rhode-Saint-Genèse, Belgium, chahine@vki.ac.be
[2] University of Oxford, Department of Engineering Science, Oxford, United Kingdom
[3] Von Karman Institute for Fluid Dynamics, Rhode-Saint-Genèse, Belgium, verstraete@vki.ac.be
[4] University of Oxford, Department of Engineering Science, Oxford, United Kingdom, li.he@eng.ox.ac.uk

1. Abstract
A multidisciplinary and multiobjective optimization of a transonic fan blade for a high bypass ratio turbofan engine is presented including aerodynamic as well as structural static and dynamic performance criteria. The optimization strategy applied is based on a two-level approach consisting of a Differential Evolution algorithm coupled to a Kriging metamodel in order to speed up the optimization process. High-fidelity performance evaluations are carried out by means of 3D Computational Fluid Dynamics and Computational Structural Mechanics analysis tools. Multiple key operating points are considered in the optimization process; aerodynamic performance is evaluated at top-of-climb and cruise conditions, while maximum stresses are evaluated at take-off operation, taking into account centrifugal and gas loads. Blade vibration is furthermore assessed over the entire operating range. Aerodynamic performance is separately evaluated for core and bypass flows in order to match the requirements specified by the engine cycle design.
2. Keywords: Multidisciplinary Optimization, Fan Blade, Turbofan, Bypass Ratio, Aerostructural Optimization.

3. Introduction
High bypass ratio turbofan engines are today the almost exclusive powerplant of choice for medium and long haul commercial aircraft due to high obtainable thrust levels combined with good fuel efficiency. About 80% of a modern turbofan engine's thrust is generated by the fan. Low engine fuel consumption requires the fan blades to transfer mechanical shaft power into thrust with the lowest possible amount of aerodynamic losses (high propulsive efficiency). Although this goal can be formulated easily, in practice additional requirements such as stable operation under widely varying operating conditions, transonic relative inlet flows and structural integrity constraints significantly complexify the design problem. Structural loads occurring during operation include centrifugal forces, aerodynamic loads and periodic blade excitations from varying sources. As the fan blade is a safety critical component, all of the above aspects need to be considered in the design process.
In the aero-structural design process commonly applied by industry, the structural and aerodynamic design are mostly handled separately from each other and the design progresses iteratively from one discipline to another until a satisfactory solution is found. The result is a lengthy and expensive design process with the additional disadvantage that interactions between the involved disciplines are difficult to reveal.
In this paper the application of a multidisciplinary and multiobjective optimization system to the above stated design problem is presented. The optimization method enables the concurrent evaluation of aerodynamic and structural performance criteria, therefore facilitating the identification of the interaction of disciplines and allowing the design to progress towards global optimal solutions in a reduced design time.

4. Baseline design
Specified engine cycle requirements are the starting point for the fan blade design process. To enable a reasonable design space definition, a baseline design was generated using two-dimensional preliminary aerodynamic design tools based on first principles and correlations. The methods enable a reasonable estimation on required spanwise blade angle distributions and suitable profiles to be made. The obtained geometry was analyzed using CFD and slightly adjusted manually to meet the operating range requirements. However, not all aerodynamic specifications could be met at the end of this design stage.

5. Optimization system
The optimization system shown in Fig. 1 is the result of more than one and a half decades of research and development at the von Karman Institute [1],[2]. The core components of the system are a multiobjective Differential Evolution algorithm (DE) [3,4], a database, several metamodels, including Radial Basis Functions,

Artificial Neural Networks and Kriging, and a high fidelity evaluation chain including a fully automatic geometry and CAD generation, automatic meshing and high-fidelity performance evaluations by Computational Fluid Dynamics (CFD) and Computational Structural Mechanics (CSM). The optimization method is based on a two-level strategy coupling the evolutionary optimization to a sequentially updated metamodel. Prior to the optimization an initial design space sampling is performed using a fractional factorial Design of Experiments containing 128 samples plus the baseline and a design at the center of the design space. Each sample is evaluated by the high fidelity evaluation chain. The resulting relationships between optimization parameters and performance are stored in a database which serves to train the first metamodel. On the next level the optimization is performed using exclusively the metamodel for the performance evaluations. Since metamodel evaluations are computationally cheap, thousands of generations can be computed by the Differential Evolution algorithm within a few minutes. However, since the metamodel predictions at early stages of the process can be expected to be rather inaccurate, eight of the best performing designs of the Pareto front predicted by the metamodel are chosen for re-evaluation by the high-fidelity evaluation chain. The results are added to the database and used to re-train the metamodel, making it more accurate in the regions where it previously predicted optimal designs. In the remainder of this paper, one loop consisting of optimization, high-fidelity re-evaluation and metamodel generation is termed an iteration. Ordinary Kriging is used as metamodel. Each performance parameter is predicted with one dedicated metamodel, which reduces prediction error and training cost. Further implementation details of the system can be found in e.g. [4],[5].

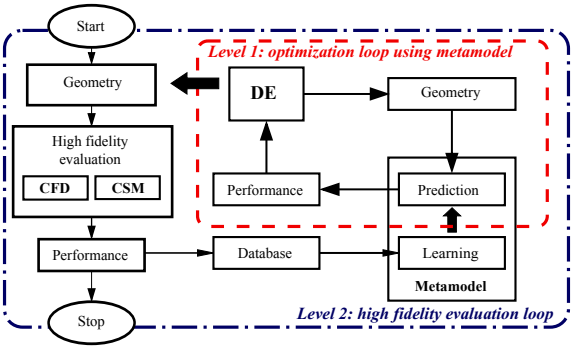

Figure 1: Flow chart of the optimization system.

6. Fan blade parametrization

The geometry of the fan blade is defined by parametric Bézier and B-Spline curves which specify the blade chord, blade angles, the thickness distributions at hub and tip sections and the profile stacking axis by lean and sweep, see Figs. 2 and 3. The blade metal angles at the leading edge, trailing edge and an intermediate point as well as the chord length are defined by spanwise B-Spline curves, as shown in Fig. 2. Control points for these distributions are defined on four spanwise positions which are being fixed for three of the points at 0, 50 and 100% span. The spanwise position of the fourth control point is added as an optimization parameter in order to allow additional control of the blade geometry close to the bypass splitter. Some of the control points are directly defined as optimization parameters and are indicated with arrows, while others are defined via geometric dependencies to other control points (e.g. angles and distances). The blade thicknesses at hub and tip sections are defined by B-Spline curves as

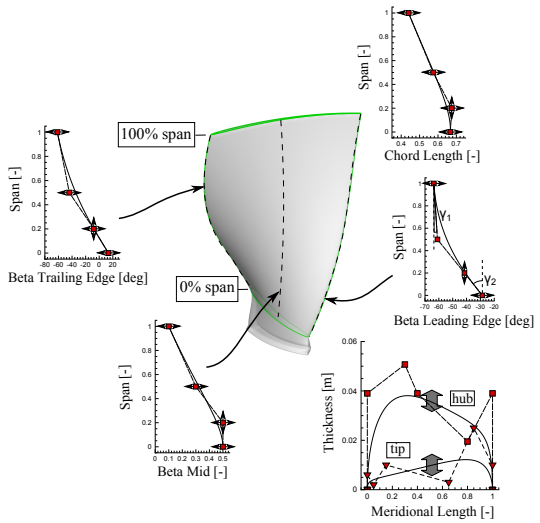

Figure 2: Parametrization of blade angles, chord length and thickness.

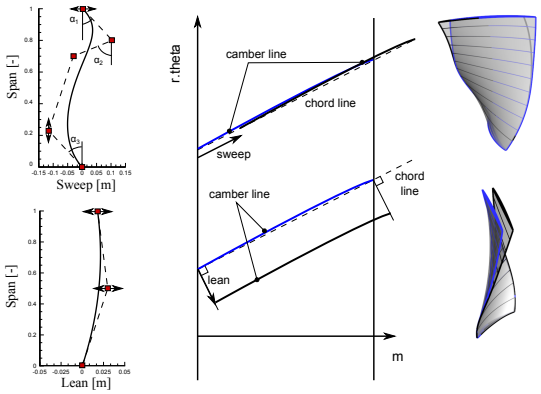

Figure 3: Lean and sweep definition and parametrization.

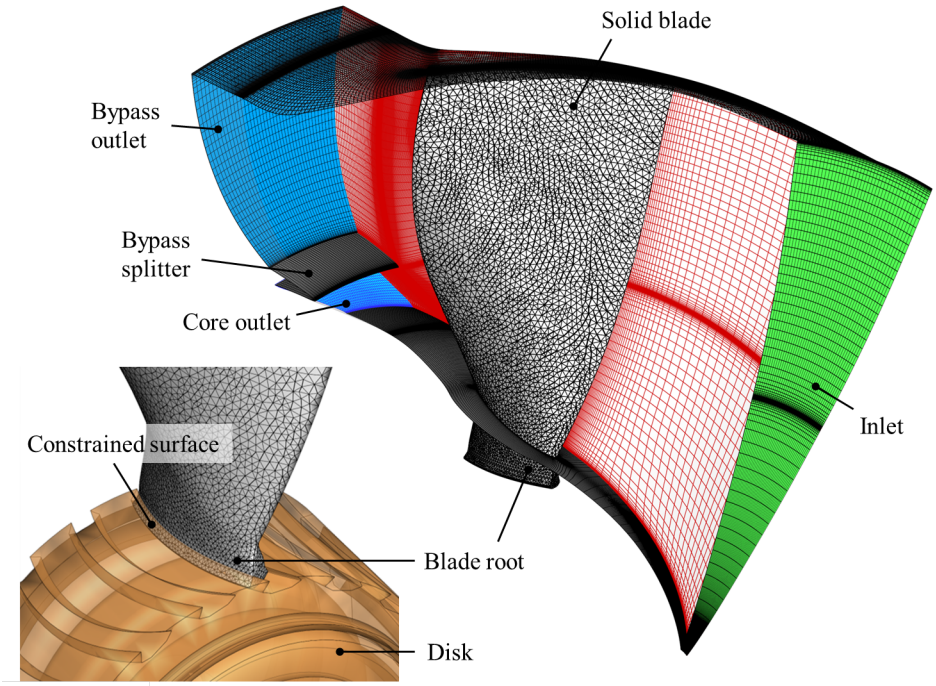

Figure 4: Computational domains of the baseline fan blade.

shown in Fig. 2 and are designed based on [6]. Both distributions can be scaled independently by a uniform scaling factor, therefore allowing thickness changes without altering the actual distributions. In addition, the number of blades is allowed to be modified resulting in a total of 26 optimization parameters.

7. High fidelity performance evaluations

The aerodynamic performance of the fan blade is assessed using the commercially available 3D Reynolds-Averaged Navier-Stokes solver FINE^{TM}/Turbo from Numeca. The solver is a structured, density based code using a finite volume method. The fluid domain is discretized using a multi-block structured mesh consisting of about 2 million grid points with a domain averaged non-dimensional height of the first cell near the wall (y+) of about 3. Turbulence effects are taken into account with the one-equation Spalart-Allmaras turbulence model.

To meet the aerodynamic design and off-design targets of the fan blade, its performance is evaluated at two key flight conditions, namely top-of-climb (ToC) and cruise. In total nine operating points are computed for each design, including four points on the top-of-climb speedline and five points on the cruise speedline. An automatic convergence check is performed after each CFD computation, which assesses the mass flow error between domain inlet and outlet and the iteration errors of isentropic efficiency and total pressure ratio. Only converged cases are subsequently assessed by an automatic postprocessing step, which extracts the required performance parameters needed by the optimizer. Non-converged cases are considered as failed and are automatically excluded from the optimization process.

The computational domains of the baseline fan blade for both solid and fluid are shown in Fig. 4. The fluid domain comprises one periodic section of the full annulus with periodic boundary conditions being applied at each side of the domain. Total pressure, total temperature, absolute inflow angle and turbulent kinematic viscosity are imposed as boundary conditions at the inlet. The low hub-to-tip radius ratio of the blade results in a transonic flow at all considered operating conditions with the relative inlet flow to the blade being subsonic for the lower part of the blade extending to about 50 percent span and supersonic for the remaining part of the blade up to the blade tip. The flow at the subsonic root section (the portion of the blade feeding the engine core) is highly sensitive towards outlet pressure differences, requiring the mass flow to be imposed as the core outlet boundary condition in order to obtain a stable flow solution. In contrast the static pressure with the radial equilibrium law is defined as boundary condition for the bypass outlet. Performance curves are computed by changing the bypass outlet static pressure.

The solid domain of the fan is discretized with an unstructured mesh consisting of quadratic tetrahedral elements. The computations are performed using the open-source finite element solver CalculiX [7]. Stresses in the blade

are computed by means of a static analysis at take-off conditions taking into account geometric non-linearities. The blade is subjected to centrifugal and gas loads whereas the gas loads are extracted from the converged take-off CFD computation of the baseline geometry and interpolated onto the FEM grid.
Additionally to the structural static evaluation, fan blade vibration is considered at all previously mentioned key operating points (take-off, top-of-climb and cruise) to assess the risk of possible high-cycle fatigue failure. Modal analysis is used to determine the natural frequencies of the fan blade while centrifugal stiffening is included in the computations in order to take into account the non-linear increase of blade stiffness with increasing rotational speed (an effect known as centrifugal stiffening). The margins between excitation frequencies and blade natural frequencies at the rotational speeds associated with the aforementioned operating points are evaluated using the Campbell diagram. Excitations from one-per-revolution and two-per-revolution disturbances are considered covering possible sources like unbalance and cross-wind. The fan blade is modelled using material properties of Ti-6Al-4V.
An important detail of the solid domain is the blade root and its restraint, which is the part of the solid extending out of the fluid domain as shown in Fig. 4. The root has important structural implications for both stresses and vibrations as it is the portion of the blade that connects to the fan disk and therefore defines the boundary conditions for the structural simulations. A typical blade-disk assembly is shown on the left bottom part of Fig. 4. In the structural computation all mesh nodes on the upper dovetail root surface are restrained in all degrees of freedom in order to simulate the disk assembly. In reality, these surfaces are in contact with the disk and small relative movements between disk and blade root are possible. Fixing the nodes will thus result in unrealistically high stress concentrations on the surface. These stresses are not taken into account in the postprocessing step.

8. Objectives and constraints

Two objectives and in total 12 aerodynamic and structural constraints are defined for the optimization problem. The objectives are defined to maximize peak efficiency at cruise rotational speed and maximize stall margin, defined as the non-dimensional mass flow difference between the cruise design point and the last converged CFD operating point towards low mass flows, see Fig. 5. The maximization problem is converted to an equivalent minimization problem, such that both objectives are stated as

$$\textbf{minimize} = \begin{cases} -\eta_{cruise,peak} \\ -\left(\frac{\dot{m}_{cruise,design} - \dot{m}_{cruise,stall}}{\dot{m}_{cruise,stall}}\right) \end{cases} \tag{1}$$

The stall margin objective implies the assumption that numerical instabilities occuring at lower mass flows resemble the physical process of stall/surge in a real fan.
The constraints are defined as follows

$$\dot{m}_{cruise,stall} \leq \dot{m}_{cruise,design} \leq \dot{m}_{cruise,choke} \tag{2}$$
$$0.97 \cdot \dot{m}_{toc,design} < \dot{m}_{eval,toc} < 1.03 \cdot \dot{m}_{toc,design} \tag{3}$$
$$\Pi_{t-t,bypass,eval,toc} > 1.7 \tag{4}$$
$$\Pi_{t-t,core,eval,toc} > 1.4 \tag{5}$$
$$Ma_{max,bypass,eval,toc} < 0.9 \tag{6}$$
$$Ma_{max,core,eval,toc} < 0.9 \tag{7}$$
$$\alpha_{max,bypass,eval,toc} < 70 \text{ deg} \tag{8}$$
$$\alpha_{max,core,eval,toc} < 70 \text{ deg} \tag{9}$$
$$\sigma_{vM} < 800 \text{ MPa} \tag{10}$$
$$\Delta\hat{F}_{cruise} + \Delta\hat{F}_{ToC} + \Delta\hat{F}_{T/O} > 12 \tag{11}$$

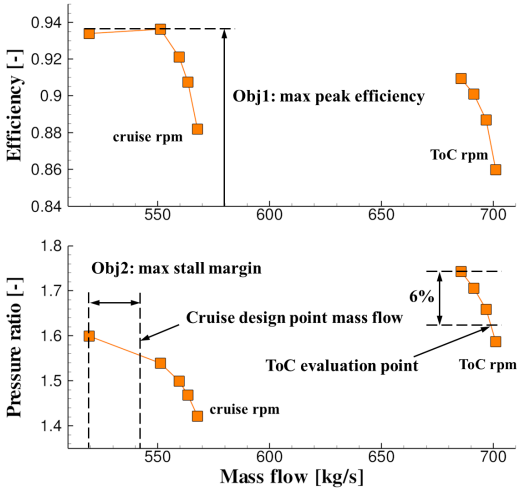

Figure 5: Definition of objectives and the top-of-climb evaluation point shown on the performance map of the baseline design.

Four constraints (Eq. (2) and (3)) are imposed to ensure that the operating range of the fan matches the engine cycle design requirements at cruise and top-of-climb defined as $\dot{m}_{cruise,design} = 541$ kg/s and $\dot{m}_{toc,design} = 699$ kg/s. A top-of-climb evaluation point with a 6% stall margin with respect to the total pressure ratio is defined as shown in Fig. 5. This is the operating point where the required total pressure ratio is the highest throughout the mission. Two constraints are therefore defined to ensure that the pressure ratios for core

and bypass flows are not lower than the design requirements, see Eq. (4) and (5). Additionally, Eq. (6)-(9) limit the maximum absolute inlet Mach numbers and the maximum absolute flow angles at the bypass and core inlet to ensure that the stators located further downstream (Outlet Guide Vane in the bypass and Engine Section Stator in the core) receive a healthy inlet flow and performance improvements of the fan blade are not obtained at the cost of overall stage performance. The absolute flow angle is measured with respect to the meridional plane. Equation (10) defines that the maximum von Mises stresses in the fan blade are required to be lower than 800 MPa, leaving a 130 MPa dynamic stress margin towards the yield stress of the titanium alloy. Blade vibration is assessed at cruise, top-of-climb and take-off. A minimum required frequency margin between the first bending mode of the blade and the first harmonic of a one and two per revolution excitation are defined as constraint (Eq. (11)).

9. Results

In Fig. 6 the objective space is shown after a total of 10 iterations. Each symbol in the plot represents a design which was evaluated by the high-fidelity evaluation chain. DOE samples are shown as circles while designs generated during the optimization appear as squares. Samples that are satisfying the constraints are shown in light blue. Improved performance is obtained towards the lower left corner of the objective space. An indication of all designs generated during the optimization is given in the upper right corner of Fig. 6. However, the designs which are satisfying all imposed constraints are located in the region marked with the red square. The main part of Fig. 6 shows a close up on this region.

As the optimization problem is highly constrained, only three designs in the DOE database initially satisfied all constraints. After nine iterations the Kriging metamodel became sufficiently accurate to guide the optimizer to the feasible region of the design space. Subsequently, all designs generated during the ninth and tenth iteration were feasible.

The best design found after 10 iterations is designated as IT010_IND001 in Fig. 6. The baseline design is shown as orange diamond to enable a performance comparison. It should again be emphasized that the baseline design violates a number of constraints and is therefore not part of the feasible set of designs. In contrast, design IT010_IND001 is satisfying all imposed constraints and at the same time shows improvements in both objectives.

A more detailed assessment of the aerodynamic performances of both designs is possible by comparing their performance maps, as shown in Fig. 7. The cruise design point mass flow is indicated by the dashed line. As shown in the lower part of Fig. 7, the pressure ratio of the fan was successfully increased over the entire operating range to meet the core and bypass pressure ratio requirements at top-of-climb. The baseline design generates overall a lower pressure ratio, which generally translates to higher obtainable efficiencies. However, with the increase in pressure ratio the optimized design still obtains a peak efficiency of 93.7%; an 0.05% improvement over the baseline design. The peak efficiency occurs at a mass flow of 561kg/s which is 0.037% above the design point mass flow. This can be deemed as reasonably close for a numerical prediction.

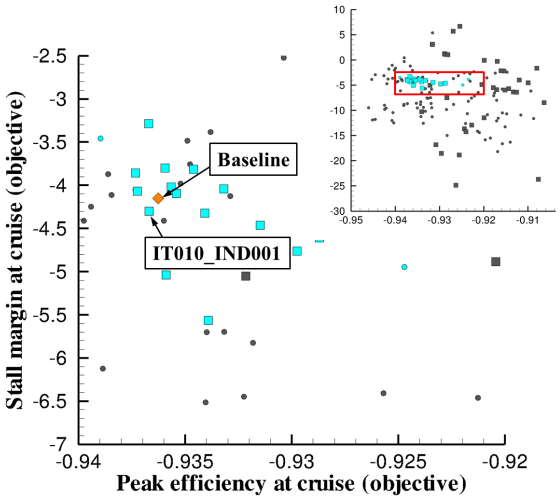

Figure 6: Objective space of the optimization after a total of 10 iterations.

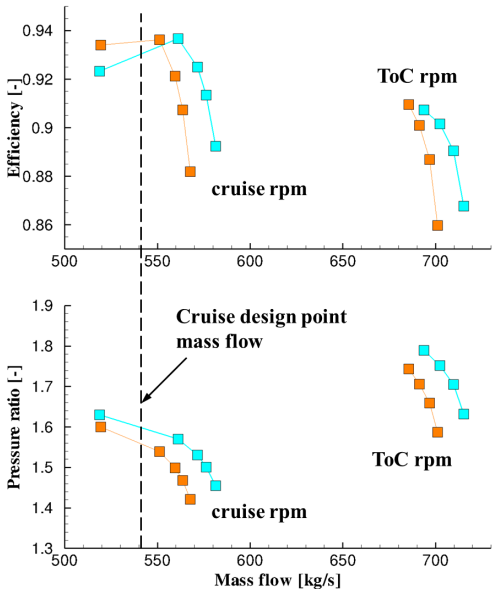

Figure 7: Comparison of performance maps of the baseline design (orange) and the optimized design (light blue).

An analysis of the optimization process reveals that the structural constraints were among the most difficult to satisfy. As the baseline design was generated purely based on aerodynamic considerations, it violated both the stress and the vibration constraints. A comparison of the von Mises stress distributions on the suction side surfaces of baseline and optimized design is shown in Fig. 8. Peak stresses exceeding the constraint value occur in the baseline design at the leading edge close to the transition to the dovetail root and on the suction side hub region close to the trailing edge (both regions are indicated by ellipses in Fig. 8). The stress levels in the critical regions were successfully lowered by the optimizer as shown on the right hand side of Fig. 8. As noted above, the high stresses in the dovetail root are not taken into account in the postprocessing step as these are artificially increased due to the boundary conditions applied in the structural computations.

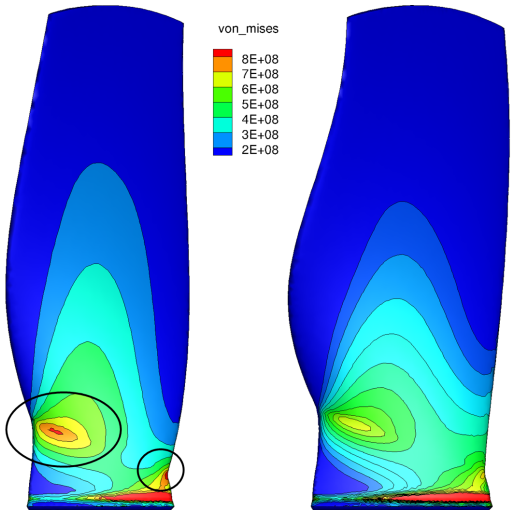

Figure 8: Von Mises stress distribution in the baseline (left) and the optimized design.

10. Conclusions

This paper presents the application of a two-level optimization system based on a Differential Evolution algorithm coupled to a sequentially updated Kriging metamodel to the multidisciplinary and multiobjective optimization of a transonic fan blade for a high-bypass ratio turbofan engine. Aerodynamic performance requirements for bypass and core sections are simultaneously taken into account in the optimization problem formulation. Stresses and vibrations are furthermore considered as structural constraints. The result is a problem with a total of 12 aerodynamic and structural constraints. The optimization system successfully identified the feasible region in the design space after 9 iterations. Subsequently, the objectives (efficiency and stall margin) were rapidly improved. The best design was found after 10 iterations, which showed an improvement of both objectives with respect to the baseline design; a significant improvement, as the baseline design did not satisfy all imposed constraints.

11. Acknowledgements

The research leading to these results has received funding from the European Union Seventh Framework Programme (FP7/2007-2013) under grant agreement no [316394].

12. References

[1] S. Pierret, *Designing Turbomachinery Blades by Means of the Function Approximation Concept Based on Artificial Neural Network, Genetic Algorithm, and the Navier-Stokes Equations*, PhD thesis, Faculté Polytechnique de Mons/ von Karman Institute for Fluid Dynamics, 1999.

[2] T. Verstraete, *Multidisciplinary Turbomachinery Component Optimization Considering Performance, Stress, and Internal Heat Transfer*, PhD thesis, University of Ghent/ von Karman Institute for Fluid Dynamics, 2008.

[3] R. Storn and K. Price, Differential Evolution - A Simple and Efficient Heuristic for Global Optimization over Continuous Spaces, *Journal of Global Optimization*, 11(4), 341-359, 1997.

[4] T. Verstraete, Multidisciplinary Optimization of Turbomachinery Components using Differential Evolution, *VKI LS 2010-07 Introduction to Optimization and Multidisciplinary Design in Aeronautics and Turbomachinery*, Rhode-Saint-Genèse, Belgium, 2010.

[5] T. Verstraete, CADO : a Computer Aided Design and Optimization Tool for Turbomachinery Applications, *2nd International Conference on Engineering Optimization*, Lisbon, Portugal, 2010.

[6] A. Wennerstrom, Design of Highly Loaded Axial Flow Fans and Compressors, Concepts ETI, 2001.

[7] G. Dhondt and K. Wittig, A Free Software Three-Dimensional Structural Finite Element Program, *www.calculix.de*.